Journal of NAMP 70, (2025) 9-20

The Nigerian Association of Mathematical Physics

Journal homepage: https://nampjournals.org.ng

MICROWAVE TOMOGRAPHY: EXPERIMENTAL SET-UP FOR 3D OBJECTS CHARACTERIZATION USING 10 GHZ MONOPOLE ANTENNAS

Bisu, A. A.
Electronics Unit, Department of Physics, Bayero University, Kano-Nigeria..

ARTICLE INFO

Article history:
Received 30/5/2025
Revised 2/6/2025
Accepted 7/6/2025
Available online 17/7/2025

Keywords:
Characterisation,
Experiment,
Frequency,
Imaging,
Microwave,
Network,
Transmission,
Tomography.

ABSTRACT

This paper explores the experimental setup for measurements and material characterisation of a 3-D objects using microwave tomography technique in a high frequency testing facility. Experiment was conducted using state-of-the art vector network analyser (VNA) with capability of operating up 1.1 THz. Monopole antennas operating at 10 GHz were used to investigate how 3-D printed objects scatter or guide the signals at high frequencies. VNA was calibrated using SOLT calibration standard before starting measurements. Experiments using 3-D objects fabricated with wood, metal, glass, and aluminium were conducted and analysed based on the scattering parameters to identify the degree of signal reflection (S_{11}/S_{33}) and transmission (S_{13}/S_{31}) in the presence of the 3-D object within the imaging area. Results showed that 3-D object fabricated with the wooden material has the highest transmission coefficient of -32 dB compared with metallic material with -52- and -53-dB transmission coefficient.

1. INTRODUCTION

Microwave tomography (MWT) is a technique that utilised radiofrequency within the microwave (3-300GHz) band of the electromagnetic spectrum to reconstruct image of an object. This is a non-invasive imaging technique that uses microwave signals to create detailed images of the internal structure of objects, including biological tissues [1]. This technique is also used for communications channel characterisation which involve studying and understanding the behaviour of channel under investigation. Radiofrequency tomography or MWT imaging was first introduced in 2010, as an alternative non-ionizing diagnostic method to assess bone health [1-5]. The key components of MWT experiment include Antenna System, Signal Processing Algorithms, and Microwave Signal Sources. An array of antennas that transmit (Tx) and receive (Rx) microwave signals form the antenna system component of the MWT experiment setup.

*Corresponding author: BISU, A A
E-mail address: aabisu.elt@buk.edu.ng
https://doi.org/10.60787/jnamp.vol69no2.535

This configuration of the antennas can vary based on the specific application and the desired imaging characteristics. The raw data collected by the antennas with the help of network analysers like Vector Network Analyser (VNA) are processed using sophisticated signal processing algorithms. Reconstruction algorithms, such as inverse problem-solving techniques are employed to convert the measured signals at specific operating frequency into an image that represents the distribution of electrical properties (dielectric constant *E*) within the object [6]. MWT systems use controlled microwave sources such as signal generator or the VNA as a source to generate the signals that interact with the target object. These sources can be designed to produce specific frequencies or a range of frequencies, depending on the imaging requirements. Image reconstruction tends to have sharper image at higher frequencies as previous studies showed that the spatial resolution of the image is proportional to the frequency (wavelength) of the signal [7]. MWT technique has applications in various fields, such as medical diagnostics, industrial testing, and material characterization [1,6, 8-13]. Communication channel characterisation that helps in designing systems that effectively transfer information regardless of the channel being perturbed with impairments like attenuation, noise, and distortion. Applications in the industry are mostly for inspection and monitoring purposes [6]. Recently, MWT are integrated with the control unit of the industrial system to increase system efficiency and processing quality [6].

This paper focused on microwave engineering that utilised the MWT to characterised 3-D objects using scattering parameters (S-Parameters) at high frequency signal. In this regard, magnitude of the signal in terms of how much gain or loss in decibels (dB) are the point of interest in our measurement. This characterisation involved the theoretical analysis and practical measurement to understand how the signal at high frequency interacts with the 3-D object/Device Under Test (DUT) based on the measured transmission and reflection of the signal during the interaction with the 3-D object made from specific material. The aim of this experiment is to contribute to designing efficient communications systems with optimal performance at high frequency. Previously, microwave imaging has been primarily based on numerical simulation data and on 2-D reconstruction. Recently, MWT imaging from 3-D experimental data been reported based on space–time beamforming [14] and tomographic reconstruction [15]. This work contributes more work on how to setup an experiment and acquire data when interacting with 3-D object within the imaging area. The 3-D microwave imaging system consists of a transmitting and receiving monopole antennas that are placed equidistance (15 cm) around a square (15cm x 15cm) imaging area. In this study, we scan the receiving antenna using an apt precision motion controller that rotate 360-deg. This was done to avoid mutual coupling when using an array of antennas.

2. Materials and Method

The experiments were caried out using state-of-the-art equipment that include a Vector Network Analyser (VNA) capable of operating up to 1.1THz with VDI-WR1.0 extenders. This is an equipment with capability of measuring complex (magnitude and phase) S-parameters that represent signal reflection and transmission. This VNA was connected to other hardware equipment and software for effective data collection and measurements as shown in figure 1. Table I summarises the equipment and software used for the experiment and measurement with descriptions. In this experiment set up, a THORLAB 3-Channel APT precision motion controller was used to control a rotational 3-D sample object holder stage through an APT server (ActiveX Control) software. Details of how the set-up was made and connections between different component of the experiment is given in the subsequent subsections.

A microwave tomography technique was used to acquire data for characterizing a solid 3-D object as a sample. Four different materials considered for the 3-D object construction are wood, metal, glass, and aluminium. The data measured was used to characterize these materials and to be use for accurate reconstruction of the 3-D object using the image reconstruction algorithms in the future work.

Table I: Summary of Experimental Hardware and Software

S/N	Name	Model	Description
1	PNA VNA	N5224A	10MHz-43.5GHz and 750GHz-1.1THz VDI WR1.0 extender capabiltiy
2	SOLT KIT	HP85033C	Content 3.5mm 50ohm Short-Open-Load-Through (SOLT) adapters for the VNA calibration
3	APT Precision Motion Controller	BSC102	THORLABS 3-Channel
4	3D Object Holder	NR360S/M	THORLABS 360-deg movable sample holder
5	APT Server (ActiveX Control) Software	V3.0.4 (2.0.6)	THORLABS ActiveX Control Software for APT precision controller
6	Antennas	10GHz	Monopole antennas operating up to 10GHz

The method employed to conduct experimental 3-D object characterization using MWT system consisted of two monopole antennas (Tx and Rx), a square (15cm x 15cm) imaging area, an APT precision motion controller (BSC102), a 3-D object stage (NR360S/M), a VNA (N5224A), and a desktop/personal computer (PC) running ActiveX software as shown in figure 1. The imaging area is an open free space containing only the 3-D object and the stage. The precision motion controller configured and activated using ActiveX control software served as a mechanical scanning system that moves the stage and the antennas (Tx and/or Rx) around the imaging area with high precision. As a result, the 3-D data acquisition was carried out effectively with flexible multiview transmitters (Tx)/receivers (Rx) on given measurement around the 3-D object to be imaged. This setup method was aimed to avoid the mutual coupling issue in an actual array. The VNA is used to collect both the incident field (the field without 3-D object in the area) and the total field (the field with 3-D object in the area) in the form of S-parameters. In this case, we used the port 1 and 3 as the active test ports in which S_{31} measurements with and without 3-D object in the imaging domain in the area (corresponding to the total field $S_{31}$and incident field S_{31}) are recorded, these parameters will be defined in subsequent section. The 3-D object samples for this experiment setup are Glass,

Aluminium, Wood, and Metal. The motion control, its scanning speed and location, and data collection by the VNA are controlled by a desktop computer.

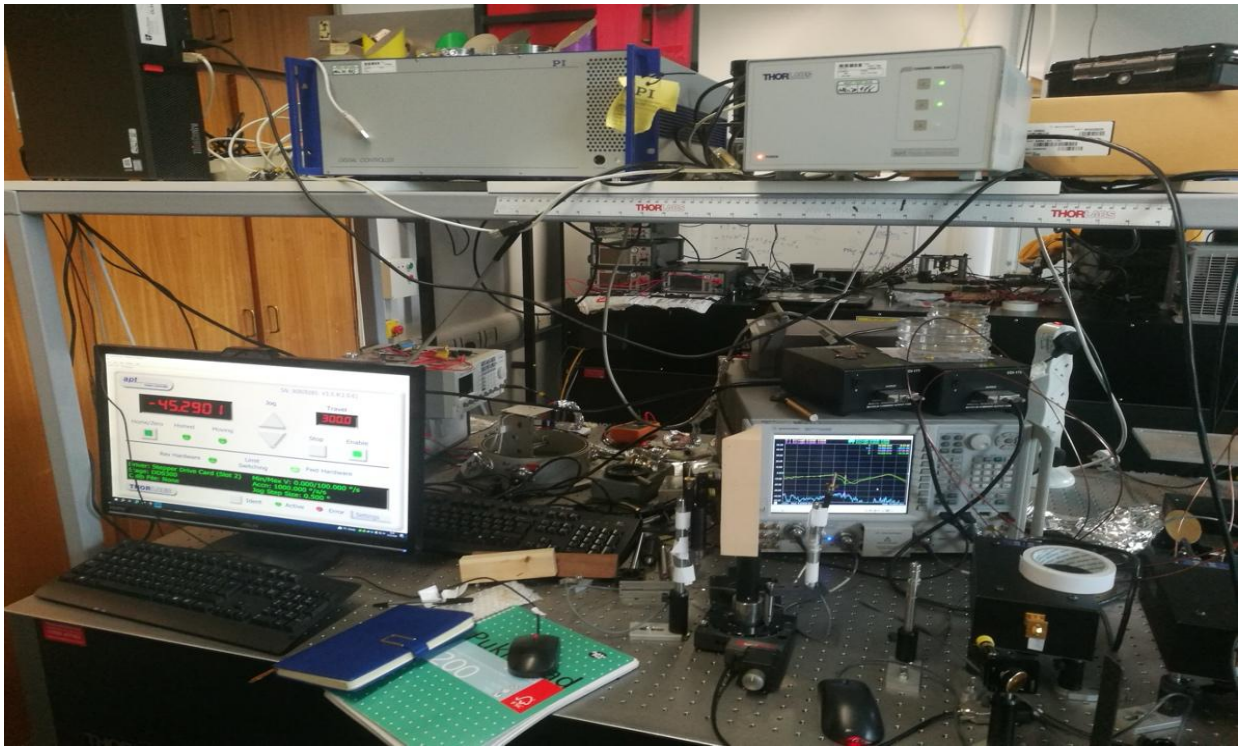

Figure 1: Experiment Setup on a THORLABS Bench

This method and MWT experimental setup have several advantages such as: (1) the coupling between multiple transmitting and receiving antennas in a typical high-resolution 3-D microwave imaging system is minimized due to the use of scanning antennas, thus simplifying the design; (2) the antenna positions are known to a high precision and (3) the system does not require switching devices as in systems containing multiple antenna array elements. Therefore, this reduces the additional noise and loss from these switching devices. However, the main disadvantage is the relatively long data acquisition time, but this is not critical and will be improved in the subsequent experiments.

2.1. Vector Network Analyser Calibrations

The Vector Network Analyzer (VNA) was calibrated using Short-Open-Load-Through (SOLT) calibration method which consists of measurements of each of the test ports (1 and 3). Specifically, a HP85033C coaxial calibration kit containing 3.5 mm SOLT adapters with 50-ohms terminations as shown in figure 2 was used. This calibration (vector error correction) removed the characterized systematic error analytically from the raw measurements (raw data) [6]. This also helps VNA to provide measurements on the DUT with an accuracy that exceed the raw performance of the VNA [6]. Considering the test ports 1 and 3, the correct (left) and noisy (errored) calibrations carried out before starting experiments with VNA is shown in figure 3. This modern calibration technique facilitates accurate measurements with minimum connections.

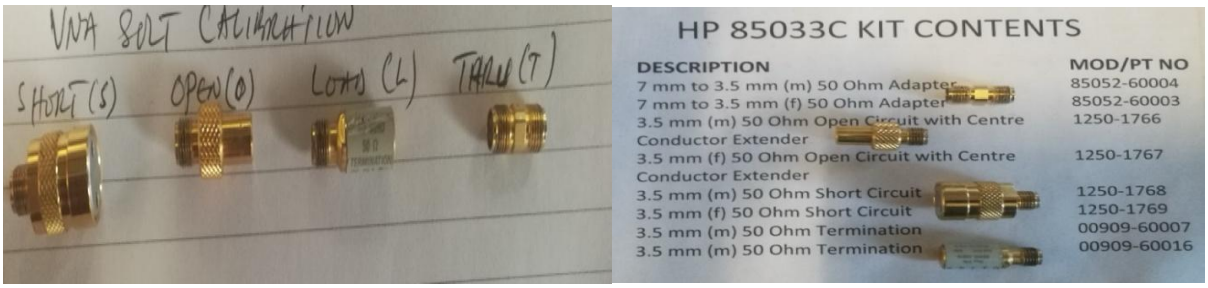

Figure 2: HP 85033C Calibration Kit Adapters Descriptions and Model

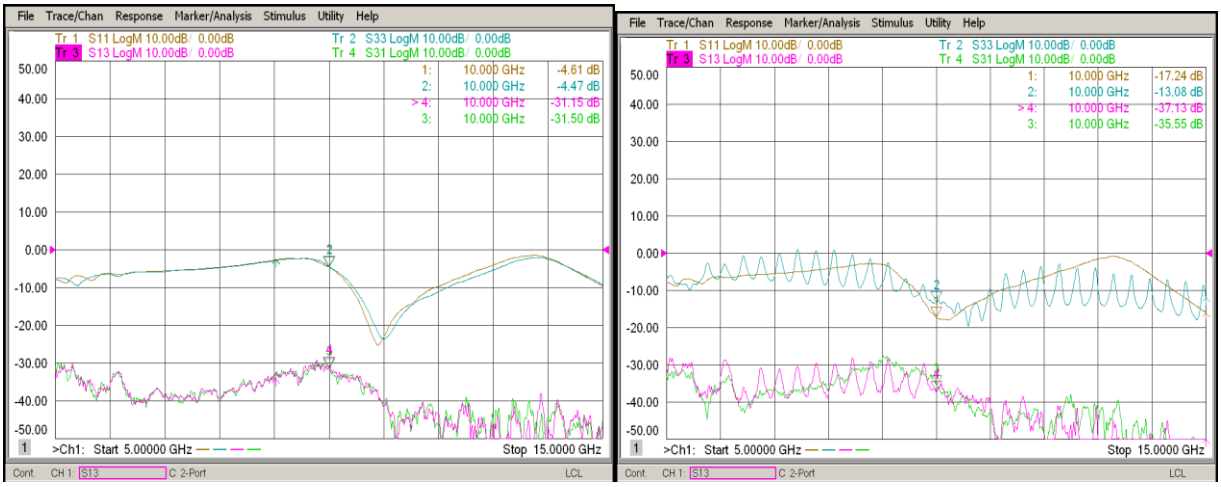

Figure 3: Good Calibration and Noisy/Error Calibration @ 10GHz

Several calibration techniques require reflection calibration for the test ports. However, SOLT is probably the best-known calibration technique that consists of a one port calibration on each test port followed by a known through (T) calibration between the test ports. The reflection calibration for each port requires three or more standards namely: an open circuit, a short circuit, and a matched 50-ohm load. In this case, we used the three standards (SOL) followed by one through (T). The frequency band of operation determines the calibration standards and test cables to be used for the calibration. Ensure not to exceed the frequency capability of the test set, cables, adapters and calibration kit. Coaxial calibration kits come in multiple versions to allow for different types of adaptors including the 3.5mm used in this calibration experiment.

2.2. Experimental Setup

This experiment was set up on THORLABS bench shown in figure 1. The APT precision motion controller and monopole antennas were mounted on the THORLABS experiment bench. The setup utilized the VNA connected to personal computer running ActiveX control software and antennas (Rx/Tx) connected to the test ports 1 and 3 using cables terminated with 50-ohms impedance as shown in figure 1.

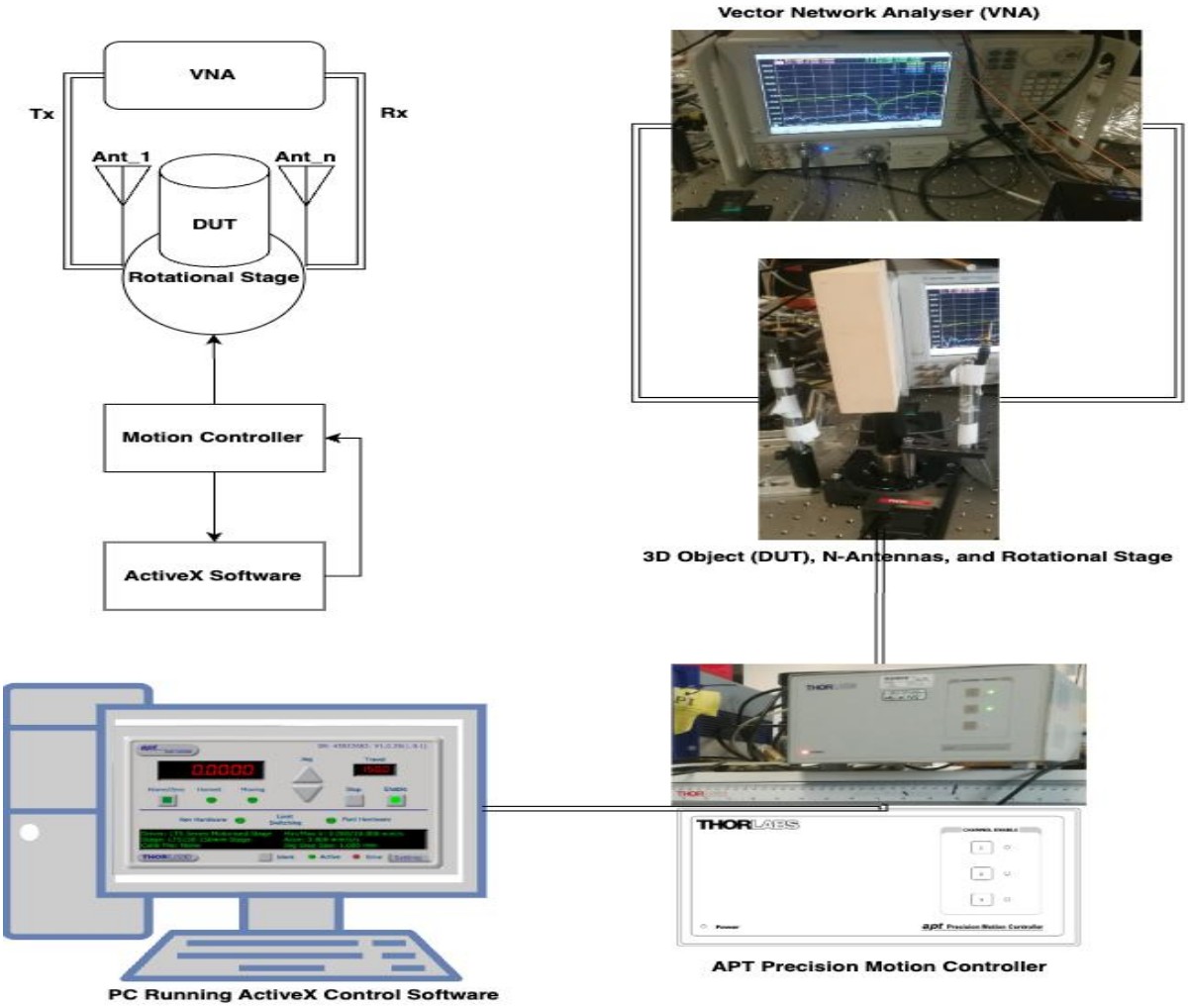

Figure 4. Flowchart (Left) and Pictorial (Right) Representation of the Experimental Setup

Figure 4 illustrates the connection between different components involved on the right and the flowchart of the signal/data traversing the system on the top left conner of the figure. This clearly showed how the data was acquired and how the component of the experimental setup is interconnected on the THORLABS bench.

3. Theoretical Framework

Microwave (MW) engineering theory was used to measure the S-parameters using the principle of 2-ports network of the VNA as shown in figure 5 and then numerically calculate the values deducted from the s-parameter matrix (1) and equations (2) to (6). These are simplified to generate the transmission (S_{13}/S_{31}) and reflection (S_{11}/S_{33}) coefficients measured from the VNA experiments.

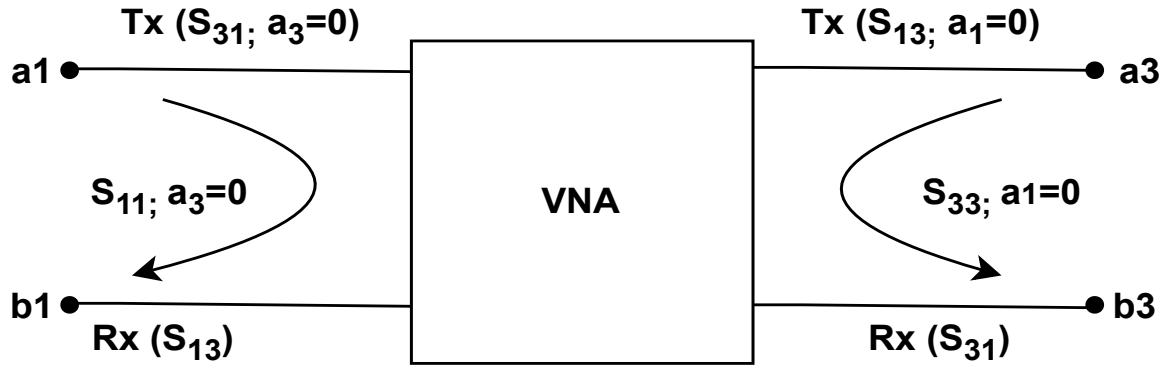

Figure 5: S-Parameters Viewed from the 2-Ports Network of a VNA with 4-Ports

Considering VNA test ports 1 and 3 as shown in figure 2 viewed from the 2-input directions of the network, the matrix in equation (1) below is determined.

$$\begin{pmatrix} b_1 \\ b_3 \end{pmatrix} = \begin{pmatrix} S_{11} & S_{13} \\ S_{31} & S_{33} \end{pmatrix} \begin{pmatrix} a_1 \\ a_3 \end{pmatrix} \qquad (1)$$

Computing and expanding the matrix in (1) will give the following equations (2) and (3)

$$b_1 = a_1 S_{11} + a_3 S_{13} \qquad (2)$$

$$b_3 = a_1 S_{31} + a_3 S_{33} \qquad (3)$$

Substituting conditions when a_1=0 (view of the input signal from port 3) and when a_3 =0 (view from port 1), equations (4) and (5) can be used to determine the S-parameters for the 2-port network shown in figure 5. Values of the reflection (S_{11}) and transmission (S_{13}) coefficients are determined from equation (2) which led to equation (4) as follows.

$$S_{11} = \frac{b_1}{a_1};\ a_3 = 0 \ \ and \ \ S_{13} = \frac{b_1}{a_3};\ a_1 = 0. \qquad (4)$$

While values of the reflection (S_{33}) and transmission (S_{31}) coefficients are determined from equation (3) as follows.

$$S_{33} = \frac{b_3}{a_3};\ a_1 = 0 \ \ and \ \ S_{31} = \frac{b_3}{a_1};\ a_3 = 0 \qquad (5)$$

Numerical values of the transmission (S_{13}/S_{31}) and reflection (S_{11}/S_{33}) coefficients obtained in equations (4) and (5) are dimensionless (i.e without unit) but usually measured in dB using the logarithmic function to base 10 as in equation (6).

$$S_{ij}(dB) = 10 \log_{10} \left\{ \frac{b_i}{a_j} \right\} \qquad (6)$$

where the value of $i, j = 1\ or\ 3$ in this case, or any value assigned to the active ports during the measurements and experiment.

Results and Discussion

Measurements were carried out experimentally to characterized different 3-D material objects including Aluminium, Glass, Metal, and Wood using reflection and transmission (S-parameters) coefficient. The results from the experimental were used to characterized 3-D objects based on the material used to make it and how signal is reflected (S_{11}/S_{33}) or transmitted (S_{13}/S_{33}) within the imaging area. The transmission coefficient (S_{13}/S_{31}) between the transmitter and receiver separated by 15 cm, is measured as a function of frequency, as shown in figures 6 to 9 [8]. The curves in these figures represent the background S_{13}/S_{31} with the 3-D objects manufactured with four different materials mentioned. It is noted that at 10 GHz, corresponding to the common frequency for the S_{11}/S_{33} parameters shown in the figures. The background S_{13}/S_{31} is approximately -4 dB for all the different materials use in making the 3-D objects, while the scattered S_{13} and S_{31} are approximately between -32 dB (wood), and -53 dB (metal). The use of a lower frequency would yield a weaker scattered field, as well as lower resolution in the image reconstruction. These used 10 GHz frequency to image and characterize 3-D objects fabricated using unique materials. Although not all of the 3-D objects in this experiment may be use for the subsequent experiment, it serves as a good test for the 3-D inverse scattering algorithm and 3-D microwave imaging experimental setup. Subsequent research will be investigating realistic 3-D objects characterization within sub-THz region and imaging by array antennas.

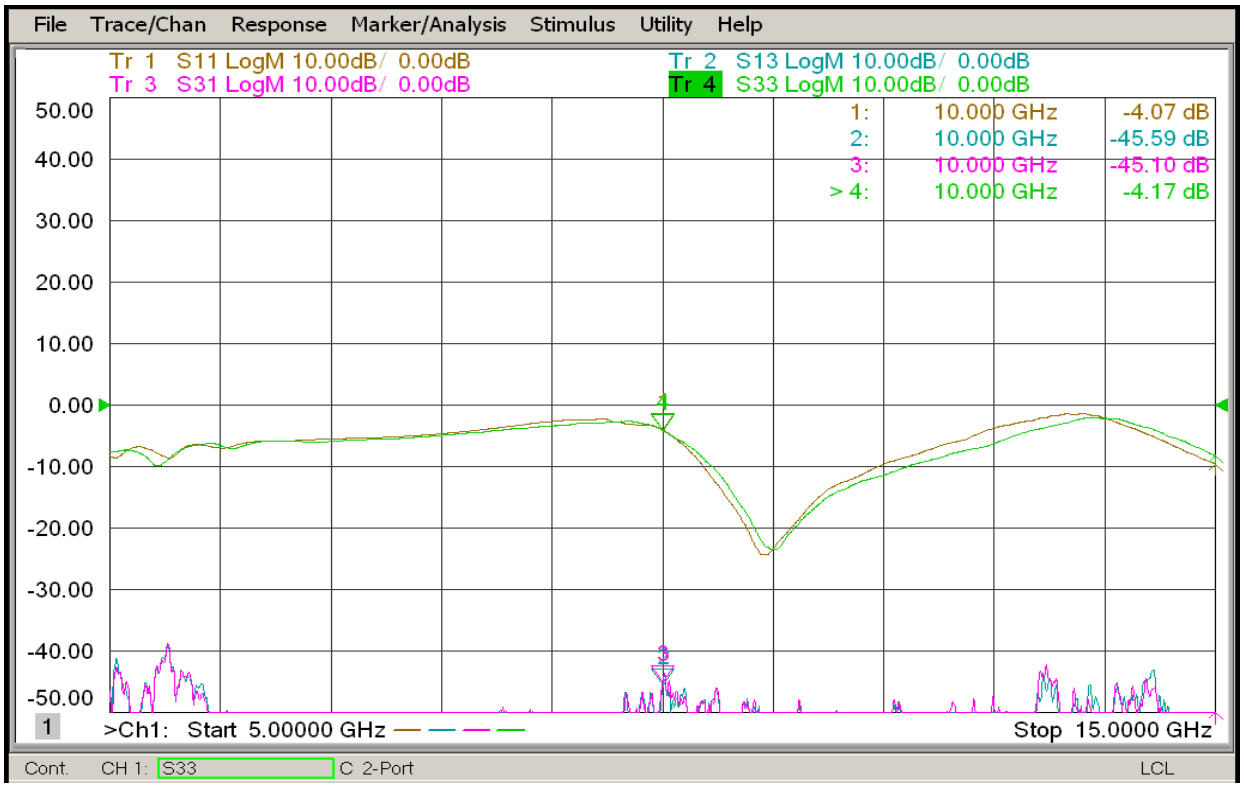

Figure 6: Transmission and Reflection measured for Aluminium at 10 GHz

The values of the transmission (S_{13}/S_{31}) and reflection (S_{11}/S_{33}) coefficient parameters measured for the 3-D object fabricated with Aluminium as shown in figure 6 indicated the lowest value of approximately -4 dB for the reflection coefficient while transmission coefficient value was found to be -45 dB. This showed that there is more signal reflection than transmission when the 3-D object material is an aluminium.

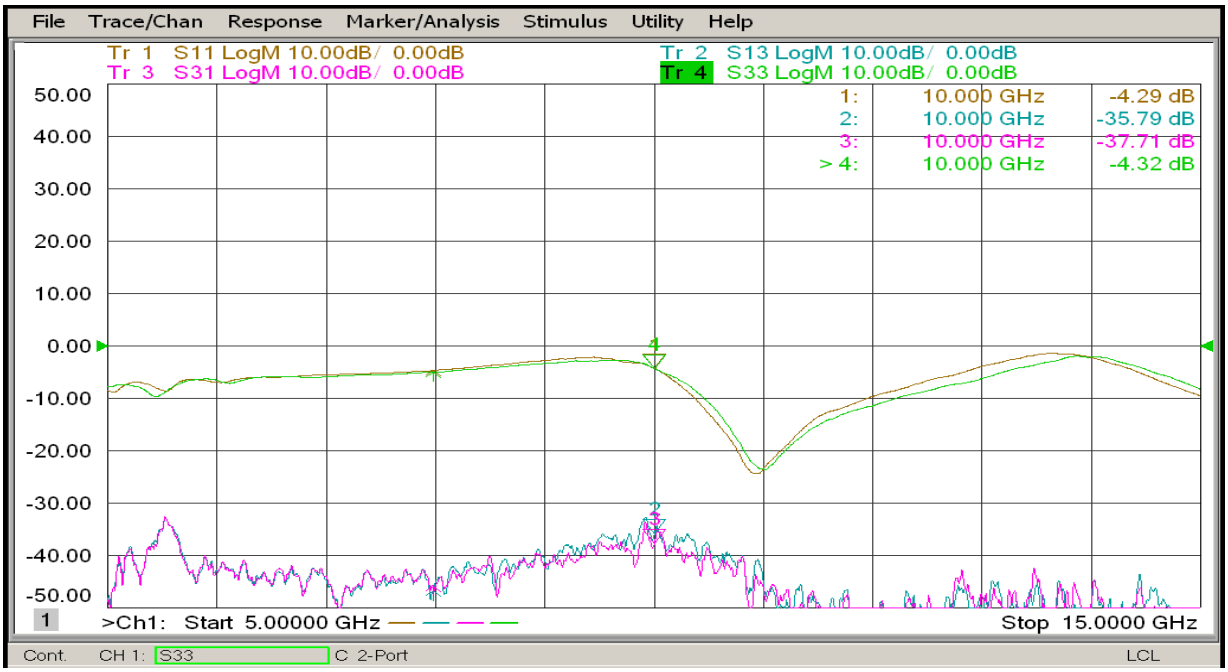

Figure 7: Transmission and Reflection measured for Glass at 10 GHz

The transmission and reflection coefficient parameters measured for the 3-D object fabricated with Glass as shown in figure 7 indicated the value of approximately -4.3 dB for the reflection (S_{11}/S_{33}) coefficient while transmission coefficient value was found to be approximately -36 dB for S_{13} and -38 dB for S_{31}. This showed that there is more signal reflection than transmission when the 3-D object material is a Glass, but this is somewhat better than aluminium in terms of transmission performance.

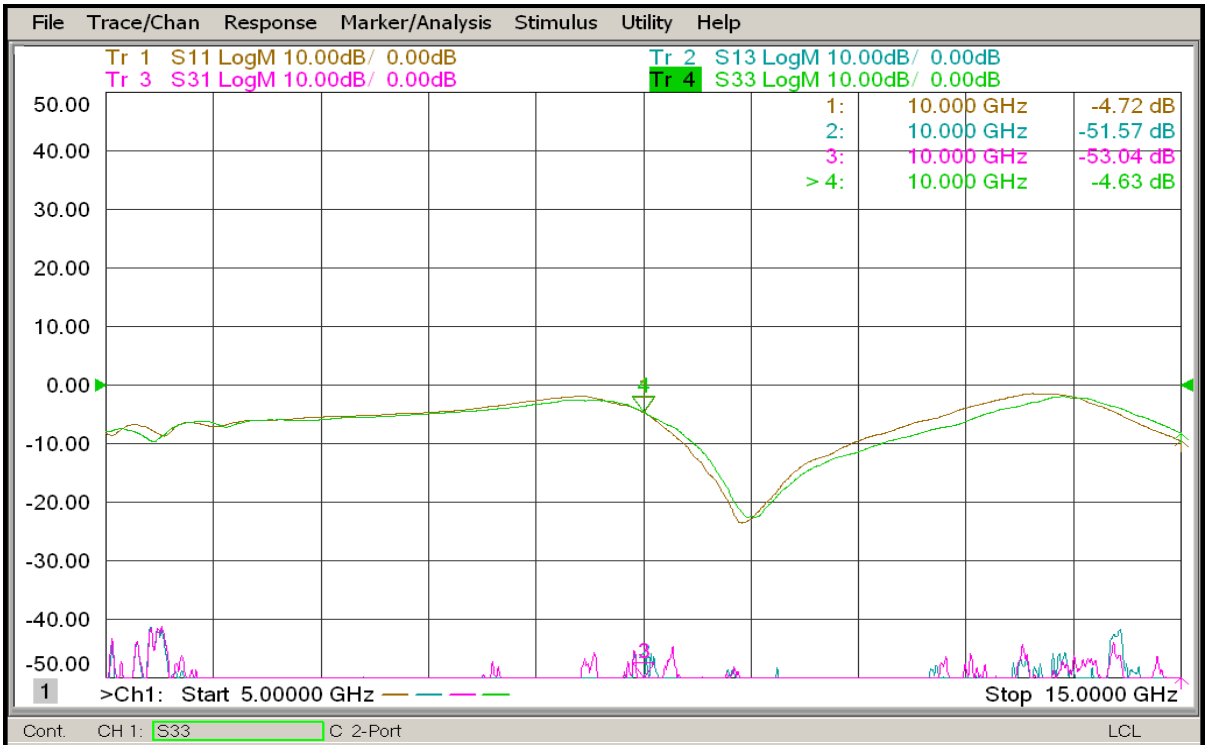

Figure 8: Transmission and Reflection Measured for Metal at 10 GHz

The transmission and reflection coefficient parameters measured for the 3-D object fabricated with Metal as shown in figure 8 indicated the value of approximately -4.7 dB for the reflection (S_{11}/S_{33}) coefficient while transmission coefficient value was found to be approximately -52 dB for S_{13} and -53 dB for S_{31}. This also indicated more signal reflection than transmission when the 3-D object material is a Metal, but this is somewhat better than aluminium and glass in terms of transmission performance.

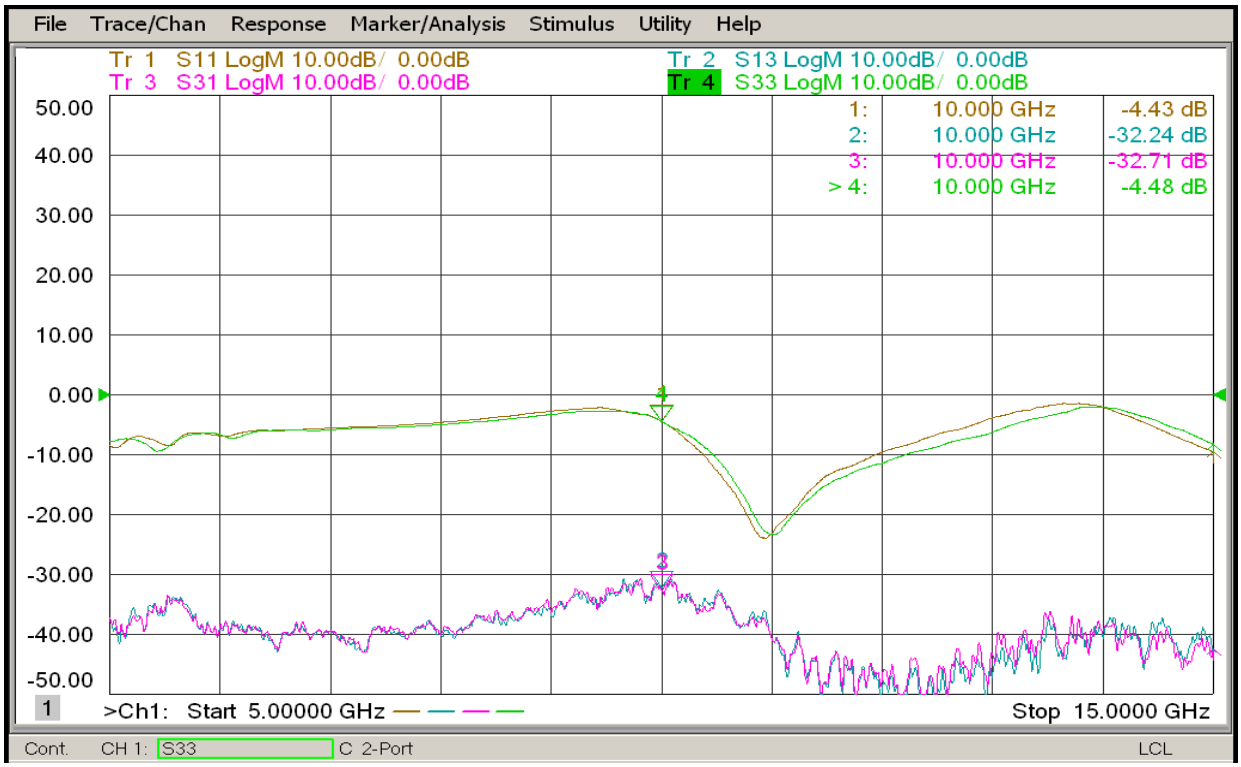

Figure 9: Transmission and Reflection Measured for Wood at 10 GHz

Lastly, the transmission and reflection coefficient parameters measured for the 3-D object fabricated with Wood as shown in figure 9 indicated the value of approximately -4.4 dB for the reflection (S_{11}/S_{33}) coefficient while transmission coefficient value was found to be approximately -32 dB for S_{13} and -33 dB for S_{31}. This also indicated more signal reflection than transmission when the 3-D object material is a Metal, but this is somewhat lower than other materials terms of transmission performance.

Overall, the results obtained and summarized in Table II showed that the strength of the transmission and reflection coefficients parameters of a 3-D objects depends on the material used for the fabrication of the object under study. Considering the magnitude of the S-parameters measured in this experiment, it was observed that more signal was transmitted (S_{13}/S_{31}) more than it was reflected by the 3-D objects under investigation as in Table I.

Table: Results Summary at 10GHz

3-D Object Material	S_{11} (dB)	S_{33} (dB)	S_{13} (dB)	S_{31} (dB)
Wood	-4.43	-4.48	-32.24	-32.71
Metal	-4.72	-4.63	-51.57	-53.04
Aluminium	-4.07	-4.17	-45.59	-45.10
Glass	-4.29	-4.32	-35.79	-37.71

Calibration	-4.61	-4.47	-31.15	-31.50

Conclusion

This paper demonstrated an experiment for 3-D object characterization using microwave tomographic imaging system and how to set up the experiment using state-of-the-art VNA. Calibration of the VNA was also carried out to reduce error to the barest minimum during the measurement as well as serving as a form of vector error correction while using the VNA for the experiment. This employed the SOLT calibration technique and used the PNA VNA as the key equipment for the measurement of transmission (S_{31}/S_{13}) and reflection (S_{11}/S_{33}) coefficients. In this system, two dipole antennas are designed to transmit and receive electromagnetic signals at 10 GHz. This technique reduced the mutual coupling of antennas and resulting in accurate measurements of scattered near-field waves. The acquired 3-D object S-parameter data were used to unravel the multiple scattering effects for four different fabrication materials. The results showed that 3-D object fabricated with the Wooden material has the highest transmission (S_{13}/S_{31}) coefficient of -32 dB compared with metallic material with -52 to -53 dB transmission coefficient. Future work includes developing a 3-D object characterisation using microwave tomographic imaging system designed for a more realistic heterogeneous communication channels and for clinical applications such as identifying brain tumour in a 3-D skull.

References:

[1] P.M. Meaney, D. Goodwin, A. H. Golnabi, T. Zhou, M. Pallone, S. D. Geimer, G. Burke, and K. D. Paulsen, "Clinical Microwave Tomographic Imaging of the Calcaneus: A First-in-Human Case Study of Two Subjects", IEEE Trans. Biomed. Eng. 59 (12), 3304–3313, 2012. https://doi.org/10.1109/TBME.2012.2209202

[2] T. Zhou, P.M. Meaney, M.J. Pallone, S. Geimer, K.D. Paulsen, "Microwave Tomographic Imaging for Osteoporosis Screening: A Pilot Clinical Study", IEEE International Conference on Engineering in Medicine and Biology, pp. 1218–1221, 2010. DOI: 10.1109/IEMBS.2010.5626442

[3] P.M. Meaney, D. Goodwin, A. Golnabi, M. Pallone, S. Geimer, K.D. Paulsen, "3D Microwave Bone Imaging", 6th European Conference on Antennas and Propagation, pp. 1770–1771, 2012. https://doi.org/10.1109/EuCAP.2012.6206024

[4] A.H. Golnabi, P.M. Meaney, S. Geimer, T. Zhou, K.D. Paulsen, "Microwave Tomography for Bone Imaging", IEEE International Symposium on Biomedical Imaging: From Nano to Macro, pp. 956–959, 2011. https://doi.org/10.1109/ISBI.2011.5872561

[5] P. Meaney, T. Zhou, D. Goodwin, A. Golnabi, E. Attardo, K. Paulsen, "Bone Dielectric Property Variation as a Function of Mineralization at Microwave Frequencies", International Journal of Biomedical Imaging, pp. 1–9, 2012. https://doi.org/10.1155/2012/649612

[6] Z. Wu and H. Wang, "Microwave Tomography for Industrial Process Imaging: Example Applications and Experimental Results".," *IEEE Antennas and Propagation Magazine,* Vol. 59, pp. 61–71, 2017.

[7] Z. Wu "Developing a Microwave Tomographic System for Multiphase Flow Imaging: Advances and Challenges", Transactions of the Institute of Measurement and Control, Vol. 37 (6) pp. 760–768, 2015.

[8] C. Yu, M. Yuan, J. Stang, E. Bresslour, R. T. George, G. A. Ybarra, W. T. Joines, and Q. H. Liu "Active Microwave Imaging II: 3-D System Prototype and Image Reconstruction from Experimental Data", IEEE Transactions on Microwave Theory and Techniques, Vol. 56 (4), pp. 991-100, 2008.

[9] K. Edwards, J. LoVetri, C. Gilmore, and I. Jeffrey "Machine-Learning-Enabled Recovery of Prior Information from Experimental Breast Microwave Imaging Data", Progress in Electromagnetics Research, Vol. 175, pp. 1–11, 2022.

[10] J. Hu, Z. Wu, H. McCann, L. E. Davis, and C. Xie "Quasi-Three-Dimensional Method of Moments for Analyzing Electromagnetic Wave Scattering in Microwave Tomography Systems", IEEE Sensors Journal, Vol. 5 (2), pp. 216-223, 2005.

[11] T. Lähivaara; R.Yadav; G. Link, and M. Vauhkonen "Estimation of Moisture Content Distribution in Porous Foam Using Microwave Tomography with Neural Networks", IEEE Transactions on Computational Imaging, Vol. 6, pp. 1351-1361, 2020. DOI: 10.1109/TCI.2020.3022828.

[12] I. Catapano, G. Gennarelli, G. Ludeno, C. Noviello, G. Esposito, and F. Soldovieri "Contactless Ground Penetrating Radar Imaging: State of the Art, Challenges, and Microwave Tomography-Based Data Processing", IEEE Geoscience and Remote Sensing Magazine, 251-273, 2022. *10.1109/MGRS.2021.3082170.*

[13] S. Mukerjee, J. Doroshewitz, J. M. Merlo, C. Oakley, L. Udpa, D. Macfarlane, E. Huff, And J. A. Nanzer "A Microwave Tomography System Using Time-Reversal Imaging for Forestry Applications", IEEE Journals of Microwaves Vol. 2 (4), 614-625, 2022. DOI: *10.1109/JMW.2022.3199194*.

[14] X. Li, E. J. Bond, B. D. Van Veen, and S. C. Hagness, "An Overview of Ultra-Wideband Microwave Imaging via Space–Time Beamforming for Early-stage Breast-Cancer Detection," *IEEE Antennas Propagation Magazine,* Vol. 47 (1), pp. 19–34, 2005.

[15] S. Y. Semenov, R. H. Svenson, A. E. Bulyshev, A. E. Souvorov, A. G. Nazarov, Y. E. Siziv, A. V. Pavlovsky, V. Y. Borisov, B. A. Voinov, G. I. Simonova, A. N. Starostin, V. G. Posukh, G. P. Tatsis, and V. Y. Baranov, "Three-Dimensional Microwave Tomography: Experimental Prototype of the System and Vector Born Reconstruction Method," *IEEE Transaction of Biomedical Engineering.*, Vol. 46 (8), pp. 937–946, 1999.

[16] T. Reveyrand, S. Hernández, S. Mons, and E. Ngoya, "SOLT and SOLR Calibration Methods using a Single Multiport "Thru" Standard Connection", 95th ARFTG Microwave Measurement Conference, pp. 1-4, IEEE, 2020. DOI: 10.1109/ARFTG47271.2020.9241365

[17] W. Luoa, A. Hu, K. Liu and X. Chen, "Study on SLT Calibration Method of 2-port Waveguide DUT", International Conference on Advanced Electronic Science and Technology, pp. 276-282, Atlantis Press, 2016.